Journal of Applied Fluid Mechanics, Vol. 14, No. 4, pp. 1065-1076, 2021.
Available online at www.jafmonline.net, ISSN 1735-3572, EISSN 1735-3645.
https://doi.org/10.47176/jafm.14.04.32010

Numerical Study on Natural Ventilation around a Burning Car inside a Tunnel

H. C. Lim†

School of Mechanical Engineering, Pusan National University, 2, Busandaehak-ro 63beon-gil, Geumjeong-gu, Busan, 46241, Republic of Korea

† *Corresponding Author Email*: *hclim@pusan.ac.kr*

(Received July 13, 2020; accepted December 2, 2020)

ABSTRACT

This study aimed to analyse the flow and temperature fields around a car on fire inside a medium-size tunnel under natural ventilation. The study used the fire dynamics simulator (FDS), which is an open-source software package, to simulate the thermo-fluidic characteristics inside the tunnel. A constant heat release rate (HRR) was assumed to ensure the release of consistent heat from the car while varying the speed of the mass flux natural ventilation. A medium-size tunnel and scaled car were modelled to simulate a realistic field environment; the car was assumed to have its primary components, including the body frame, tyres, seats, and other flammable materials. The constant HRR was set at 3.8 MW , which was measured in a field experiment using a cone calorimeter. The closed car windows were set to break when the temperature around them reached 600°C. Additionally, natural ventilation was one of the parameters used in the calculation; it was assigned as an inlet condition, referred to as the steady longitudinal inlet velocity, and ranged from 1.8 to 3.0 m/s. Based on the ventilation velocities, the variations of the flow characteristics, temperature field, turbulence kinetic energy levels, and vortex structure inside the tunnel were investigated. Additionally, the critical longitudinal velocity for natural ventilation was estimated by performing the current simulation under different ventilation velocities. Given that the thermo-fluidic parameters and geometry information are all similar, the FDS results were compared to those from three semi-empirical models for predicting critical ventilation velocities from previous studies.

Keywords: Tunnel fire; Natural ventilation; Car fire; Critical velocity; Smoke.

NOMENCLATURE

C	constant visibility factor
C_p	specific heat capacity
D_α	diffusivity of species α
e	enthalpy
f_b	drag force exerted by the subgrid-scale particles and droplets
Fr	Froude number
h	enthalpy
h_s	sensible enthalpy of the gas
HRR	dimensionless heat release rate
$I_b(x)$	source term
$I(x,s)$	solution of the radiation transport equation
k	thermal conductivity
K	light extinction coefficient
$\kappa(x)$	absorption coefficient
$\dot{m}_{\alpha'''}$	mass production rate of the lumped species
$\dot{m}_{b,\alpha}''''$	production rate of species α by evaporating droplets or particles
$\bar{p}$	background (thermodynamic) pressure
$\tilde{p}$	perturbation pressure
Pr_t	turbulent Prandtl number
$\dot{q}'''$	heat release rate per unit volume from a chemical reaction
$\dot{q}_{b''}$	energy transferred to subgrid-scale droplets and particles
$\dot{q}''$	conductive, diffusive, and radiative heat fluxes
$\dot{q}_r''$	radiative heat flux
Q'	dimensionless heat release rate
ρ_a	density of the ambient air in the tunnel
S	visibility
Sc_t	turbulent Schmidt number
	viscous stress

T_a	temperature of the ambient air in the tunnel
$\bar{u}$	average value of u at the grid cell centre
$\hat{\bar{u}}$	weighted average of u over adjacent cells
u_c	critical velocity
u'	physical critical velocity
Z_α	mass fraction

1. INTRODUCTION

In the last few decades, public concerns owing to several tunnel fires have increased. Some of these tragic incidents include the tunnel fire at Mont Blanc of the France and Italy border in 1999 (Vuilleumier *et al*. 2002), the Tauern tunnel fire at Austria in 1999 (Leitner 2001), the Daegu metro fire (2003) in South Korea (Hong 2004), and the Burnley tunnel fire (2007) in Austria (Beard 2009); details of other accidents can be found in the works of Beard and Carvel (2005) and H. Ingason *et al.* (2015).

Unlike other surroundings, tunnels are narrow spaces. When a car catches fire in a tunnel, it spreads in five mechanisms. (Rew and Deaves1999) The first mechanism is the flame and smoke impingement. This is caused by a low ventilation rate; the flames and smoke are deflected by the ceiling, mainly in the direction of the ventilation flow. They visually move along the ceiling above the vehicles. This process seems simple; however, it involves a complex flow interaction in terms of turbulence and chemical reactions. The second mechanism is surface spread, which involves the spreading of the flames across the surface of the fire load. The third, fourth, and fifth mechanisms are remote ignition, fuel transfer, and explosion, respectively. These three cases are results of the initial fire, fuel leakage, and explosion of fuel tanks, respectively, which are closely relevant to chemical reactions and explosions.

According to a previous report (Jones *et al.* 1987), the most common cause of death in fires is toxic gas inhalation. In fact, toxic gas inhalation causes acute respiratory distress syndrome and respiratory failure. Moreover, the flame and smoke reduce visibility in the tunnel, which limits the effectiveness of firefighting, and makes it difficult to escape (Kim *et al.* 2010). Smoke in tunnel fires has resulted in a significantly large number of casualties and loss of property. Therefore, controlling the smoke in tunnel fires can not only reduce the concentration of toxic smoke gases but also enhance visibility to help trapped people and firefighters see the way out, as well as identify the origin of the fire. Therefore, the design of longitudinal ventilation systems has been essential in tunnel safety engineering (Weng *et al.* 2015)

Two kinds of ventilation systems are generally used in tunnels: natural, and mechanical or forced ventilation. Forced ventilation systems require a huge space for installation, making it difficult for them to meet the requirements in the field, typically, in the case of poor management or maintenance. Conversely, because natural ventilation systems only require minimal expenses for maintenance, they are relatively popular, suitable for use, and relatively stable in daily operations. (Iqbal and Chan 2016; Muhic and Mazej 2014; Huang *et al*. 2006)

Natural ventilation systems utilize the wind and buoyancy force to draw in fresh air and appropriately distribute it in structures and buildings for the benefit of the occupants. Critical ventilation velocity plays a significant role in the ventilation system for the proper ventilation of the flow. It is defined as the minimum ventilation velocity inhibiting the reverse flow of smoke so that it stops the spread of the flames and smoke to the upstream region in the tunnel. Therefore, the deadly flames and smoke can be driven to one end on the condition that the ventilation velocity is not less than the critical velocity. A number of research scholars have conducted studies in this area and proposed some models for predicting the critical velocity of ventilation.

To estimate the critical velocity, Thomas (1968) suggested an equation related to the Froude number. A scaled-down fire test was created, which delineated an empirical model predicting the ratio of the heat release rate (HRR) to the critical velocity. (Oka and Atkinson 1995) Conversely, Atkinson and Wu 1996 revised an existing model based on the shape of the tunnel and proposed revised correlation factors of the tunnel shape. Additionally, the tunnel height was re-modelled based on the hydraulic diameter to propose a better prediction model (Wu and Barkar 2000). A semi-empirical model was also proposed to estimate the length of the back-layer as well as the critical velocity (by Hu *et al.* 2008; Li *et al.* 2010).

Full-scale experiments would certainly yield more reliable information on the basic environment of fire generation, growth, propagation, and extinction; however, they are substantially costly and relatively risky. Conversely, fire simulation based on artificial calculation, i.e., computational fluid dynamics (CFD), which is a less expensive method, has been used to visualize and study the fundamental physics of fire. The fire dynamics simulator (FDS), which is one of the CFD packages, is applied for fire simulation in the current study to calculate and evaluate the flame and heat transport, as well as the smoke coming from the fire. The method can numerically solve Navier–Stokes equations in incompressible, low-speed, and thermally-driven flow conditions, based on a large eddy simulation (LES) model. It is also possible to carry out a direct numerical simulation if the underlying numerical mesh is sufficiently fine. Particularly, the FDS has been known as a software for handling fire-related problems (Wen *et al*. 2007; Hwang and Edwards 2005; Lee and Ryou 2006; Liu *et al*. 2019), such as

temperature, velocity, smoke movement, and concentration distribution.

The aim of this study is to investigate the effect of car fires on thermo-fluidic variations under different ventilation conditions in a medium-size tunnel. The contents are primarily fivefold. Section 2 presents the governing equations used to solve the thermo-fluidic variation inside the tunnel and the detailed geometric and boundary conditions of a car model and tunnel domain. In Section 3, semi-empirical equations for predicting the critical ventilation velocity are introduced. Section 4 presents the numerical simulation results and discussion. Finally, the concluding remarks are presented in Section 5.

2. CFD NUMERICAL MODELLING

2.1 FDS

The FDS has been regarded as a practical tool for simulating fire behaviour and evaluating the performance of fire protection systems in tunnels. It numerically solves Navier–Stokes equations for incompressible, low-speed, thermally-driven flow conditions, which include the transport equations of mass, energy, and momentum (McGrattan *et al.* 2013). In the FDS, air and chemical reaction products are referred to as lumped species. The lumped species is simply an equivalent gas species that represents a mixture of gases that are always transported together in the same ratio, i.e., the lumped species have a single set of transport properties and react together. For instance, standard air in the atmosphere can be considered as lumped species consisting of 79% nitrogen, 21% oxygen, and trace amounts of other gases. Therefore, the transport equation of mass for lumped species can be expressed as

$$\frac{\partial}{\partial t}\left(\rho Z_\alpha\right)+\nabla\cdot\left(\rho Z_\alpha \mathbf{u}\right) = \nabla\cdot\left(\rho D_\alpha \nabla Z_\alpha\right)+\dot{m}_{\alpha'''}+\dot{m}_{b,\alpha}{}'''' \tag{1}$$

where Z_α and D_α denote the mass fraction and diffusivity of species α. The term $\dot{m}_{\alpha'''}$ denotes the mass production rate of the lumped species, and $\dot{m}_{b,\alpha}{}''''$ is the rate of production in species α in terms of evaporating droplets or particles. The terms on the right-hand side represent the source indicating the inclusion of the mass arising from the evaporation of droplets or other particles representing the small droplets from sprinkler and fuel sprays, plants, and small, unresolvable matter.

Owing to the low Mach number approximation in the FDS, the pressure can be divided into spatially and temporally resolved properties, such as thermodynamic (background) pressure $\bar{p}$ and perturbation pressure $\tilde{p}$ (Rehm and Baum 1978). The background pressure can be derived from the equation of state (ideal gas law):

$$\bar{p}=\rho RT\sum_\alpha \frac{Z_\alpha}{V_\alpha}\equiv\frac{\rho RT}{\bar{V}} \tag{2}$$

Another derivation from the low Mach number approximation is that the enthalpy h and internal energy e are related to the thermodynamic pressure: $h=e+\bar{p}/\rho$. Therefore, the transport equation of energy can be written as

$$\frac{D}{Dt}\left(\rho h_s-\bar{p}\right)+\nabla\cdot\left(\rho h_s \mathbf{u}\right) = \dot{q}'''+\dot{q}_{b'''}+\dot{q}_{r'''}-\nabla\cdot\dot{\mathbf{q}}'' \tag{3}$$

where the term $\dot{q}'''$ denotes the HRR by unit volume owing to a chemical reaction. Conversely, $\dot{q}_{b'''}$ indicates the energy transferred to small-scale droplets and particles. In the equation, the sensible enthalpy (h_s) is delineated as a mass-weighted average of the enthalpy in the lumped species. In the equation, the term $\dot{q}''$ denotes the heat flux by conduction, diffusion, and radiation as follows,

$$\dot{q}''=-k\nabla T-\sum_\alpha h_{s,\alpha}\rho D_\alpha \nabla Z_\alpha+\dot{q}_r{}'' \tag{4}$$

where k is the thermal conductivity and $\dot{q}_r{}''$ denotes the radiative heat flux.

Combustion and radiation are also important in the FDS calculation; the governing equations should include them in terms of the source terms $\dot{q}'''$ and $\dot{q}_{r'''}$ in the energy transport equation. The HRR by unit volume is described as the sum of the respective heats of formation multiplied by the mass production rates of the lumped species

$$\dot{q}'''=-\sum_\alpha \dot{m}'''\Delta h_{f,\alpha} \tag{5}$$

The net contribution of thermal radiation in the energy equation is defined as

$$\dot{q}_{r'''}=-\nabla\cdot\dot{q}_{r''}(x)=\kappa(x)\left[U(x)-4\pi I_b(x)\right]$$
$$U(x)=\int_{4\pi} I(x,s')ds' \tag{6}$$

where $\kappa(x)$ and $I_b(x)$ are the absorption coefficient, and source term, respectively, and $I(x,s)$ is the solution of the radiation transport equation in non-scattering grey gas

$$s\cdot\nabla I(x,s)=\kappa(x)\left[I_b(x)-I(x,s)\right] \tag{7}$$

The momentum transport equation can be written as

$$\frac{\partial \mathbf{u}}{\partial t}-\mathbf{u}\times\omega+\nabla H-\tilde{p}\nabla(1/\rho) = \frac{1}{\rho}\left[(\rho-\rho_0)\mathbf{g}+\mathbf{f}_b+\nabla\cdot\tau\right] \tag{8}$$

where f_b denotes the drag force applied to the sub-scale particles and droplets; τ and $\tilde{p}$ v denote the

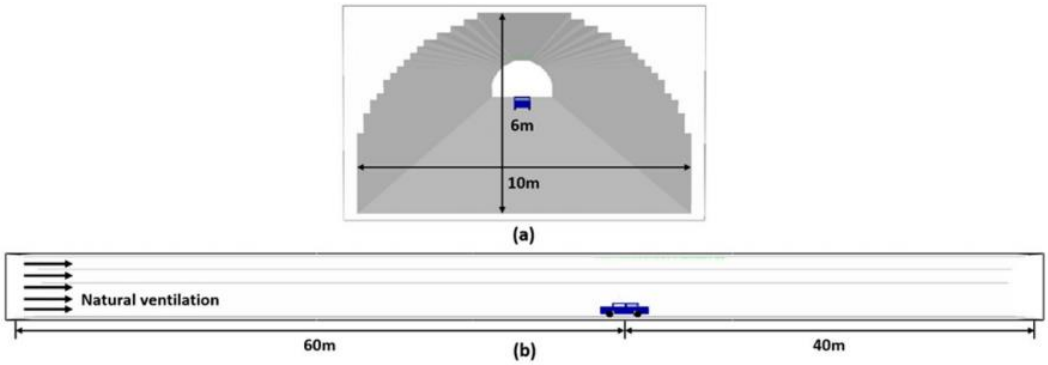

Fig. 1. Schematics of the FDS simulation indicating the tunnel and car model: (a) tunnel view; (b) side view.

viscous stress and perturbation pressure, respectively.

In this study, the LES model is used for simulating turbulent flow. Filtering is applied to separate the large-scale and sub-scale eddies; particularly, a specific filter width is adopted for the low-pass filter. In the FDS, this width of the filter is set as one-third of the cell volume, $\Delta = (\delta x \delta y \delta z)^{1/3}$. Additionally, a variation of Deardorff's model (Deardorff 1980) is applied to calculate the sub-grid turbulent viscosity.

$$\mu_t = \rho C_v \Delta \sqrt{k_{sgs}}, \quad k_{sgs} = \frac{1}{2}\left((\bar{u}-\hat{\bar{u}})^2 + (\bar{v}-\hat{\bar{v}})^2 + (\bar{w}-\hat{\bar{w}})^2\right) \tag{9}$$

where $\bar{u}$ is the average value of u at the centre-cell of the grid, and $\hat{\bar{u}}$ is the weighted average of u over the adjacent cells. Further, the model constant is set as $C_v = 0.1$.

Other diffusive parameters, such as the mass and thermal diffusivity, are related to the turbulent viscosity by

$$k_t = \frac{\mu_t C_p}{Pr_t}, \quad (\rho D)_t = \frac{\mu_t}{Sc_t} \tag{10}$$

where Pr_t (turbulent Prandtl number) and Sc_t (turbulent Schmidt number) are assumed to be constant for a given event, and are set as $Pr_t = 0.5$, and $Sc_t = 0.5$.

2.2 Configuration of Tunnel Domain

This study carried out a fire simulation using the FDS, an open-source software package, to observe fire generation and propagation in a medium-size tunnel with an arched roof under natural ventilation. The tunnel wall was assumed to be no-slip and made of concrete. The computational domain was set to a length, width, and height of 100 m, 10 m, and 6 m, respectively. The cross-sectional area and perimeter of the tunnel were 50.16 m^2 and 32 m, respectively. To simplify the problem, the car model was placed 60 m and 40 m from the left portal and right portal of the tunnel, respectively. According to the literature (see McGrattan *et al*. 2013), the initial sizing of the mesh cells should be achieved by evaluating the non-dimensional expression $D^*/\delta x$, where δx is the nominal size of a mesh cell and D^* is the characteristic fire diameter. For the desired HRR of 30 MW, D^*= 3.8 in this case, cell sizes should fall between 0.23m and 0.92m. Therefore, a cell size of 0.40m is chosen as an initial setting. Because the range above is simply a guideline, a mesh sensitivity analysis was also performed for mesh sizes of 0.20m, 0.25m and 0.80m.

As shown in Fig. 1, the tunnel surface is defined as solid obstructions. The underlying grid was assumed to be a simplified type of the immersed boundary method. The left portal of the tunnel was set as the `SUPPLY' as an inlet boundary condition (i.e., inlet condition), which is assumed to be the atmosphere that sometimes has a natural ventilation flow with a longitudinal velocity of uniform amplitude and minimal turbulent intensity. The right portal of the tunnel was set as `OPEN' to provide an open boundary condition, which indicates a non-solid and free boundary in the domain that makes the working fluid cross freely through the boundary. Regarding open boundaries, the mass fraction of the species and temperature possess their own values from the exterior when the flow comes from the inlet, and have the value of the grid cell close to the boundary when the flow comes out.

2.3 Model Configuration – a Passenger Car

To simulate an appropriate fire from the model (i.e., car), the configurations should be defined in detail. The main components inside the car model were assumed to include a body frame, tyres, seats, and other flammable materials as shown in Fig. 2. The main body measurements in terms of length, width, and height were 4.8 m, 1.8 m, and 1.4 m, respectively. The burning spot was located on a seat in the car, which was approximately 0.8 m above the floor; it was made of fabric, polypropylene, and polyurethane. In the simulation, the main materials of the car body frame, tyres, seats, and windows were assumed to be aluminum, rubber, and tempered glass, respectively. To simplify the car

model, the car shape had sharp-edged corners and rectangular windows. The windows were also assumed to break at 600 °C, which meant that the abrupt breaking of the window would be triggered when the temperature reached this value. Initially, the boundary conditions of the windows were not easy to define because the windows on the 1st-row seats (i.e., front seats) were wide open, whereas the rest of the windows remained closed. Considering the resolution, the shape of the tyres were simply considered non-circular. In spite of the limitations, the present geometry was sufficient to evaluate the effect of the car fire. Equi-spaced points of 0.1 m were used to detect the velocity, pressure, and temperature; the red points on the windows were used to measure the temperature.

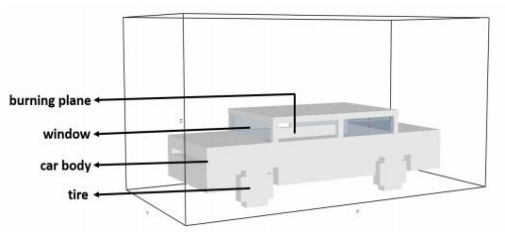

Fig. 2. Schematic of the car model in FDS.

A similar case field experiment was used as the benchmark. During the experiment, the physical engine and accessories were totally dismantled to avoid risk circumstances, and the HRR values were logged using a conical shape calorimeter, as shown in Fig.3. It was found that carrying out an in-depth analysis was quite complicated and difficult, owing to the variation of the HRR values. This study only focused on the thermo-fluidic variation around the car fire inside a medium-size tunnel. From an engineering point of view, the HRR used in the FDS simulation was fixed at 3.8 MW , which is the maximum value obtained from the field experiment. This constant HRR was expected to release consistent heat from the inside of the car. In this study, the total simulation time was set as 1000 s, and the fire started in the tunnel after 300 s.

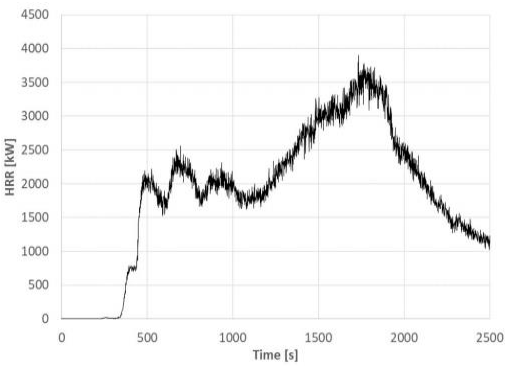

Fig. 3. HRR values measured in the car fire field experiment.

3. THERMO-FLUIDIC MODELLING

3.1 Modelling of Critical Velocity

Fire inside tunnels has always been a substantial threat. Particularly, large amounts of toxic fumes and smoke make the operation of firefighters and evacuation of people quite difficult. The rapidly increasing temperature is another threat in the limited space of the tunnel. Suitable ventilation techniques such as eliminating back-layering and driving the smoke downstream are necessary for proper ventilation. Two different techniques have been used to predict the critical velocity for ventilating the internal flow in the tunnel. The first technique is to observe the law of conservation in terms of the Froude number, and the other is to observe the law of similarity based on the dimensionless analysis. Both techniques should be validated by empirical data.

Hu *et al*. (2008) formulated a semi-empirical model predicting the back-layering length and critical velocity based on the Froude number. Their model applied the empirical equation by Kurioka *et al*. (2003) for predicting the maximum smoke temperature inside the tunnel. In the results, the HRR is closely related to the Froude number. In the full-scale tunnel data in a tunnel under a pool fire of 3.2 MW , the temperature variation has an exponential dependency, which could be used to estimate the length of back-layering. As the longitudinal ventilation velocity increases, the back-layering length gradually reduces to a point known as the critical velocity where no back-layering occurs as follows,

$$u_c = \left[g\gamma C_k H Q'^{2\varepsilon/3} (gH_d)^{\varepsilon/3} \right]^{3/(2\varepsilon+6)} \tag{11}$$

where C_k is empirically determined to be within the range 0.18 -- 0.37, C_k H_d is the distance between the tunnel height and fire spot, and g denotes the gravitational acceleration. Additionally, γ and ε are defined as

$$\begin{cases} \gamma = 1.77, \varepsilon = 6/5 & \textbf{for } Q'^{2/3} / Fr^{1/3} < 1.35 \\ \gamma = 2.54, \varepsilon = 0 & \textbf{for } Q'^{2/3} / Fr^{1/3} \geq 1.35 \end{cases} \tag{12}$$

where $Q' = Q / \left(\rho_a C_p T_a g^{1/2} H_d^{5/2} \right)$ is the dimensionless heat release rate, and $Fr = u^2 / (gH_d)$ is the Froude number. The terms ρ_a and T_a denote the density and temperature of the ambient air in the tunnel, respectively, and C_p represents the specific heat capacity.

Some researchers formulated prediction models based on dimensionless analysis and the tunnel experiment (Li *et al*. 2010; Wu and Barkar 2000). The value of the critical velocity was suggested based on the HRR. Particularly, Wu and Barkar (2000) made a variety of tunnel measurements to observe the effect of tunnel geometry on the critical velocity. In the tunnel test, they tried to make the

models have the same height but different cross-sectional geometries. For an appropriate simulation, they assumed that the tunnel had a hydraulic diameter, which was four times the tunnel cross-sectional area divided by the tunnel perimeter. The dimensionless critical velocity is also given as

$$\begin{cases} 0.4\left(\dfrac{Q'}{0.2}\right)^{1/3} & Q' \le 0.2 \\ 0.4 & Q' > 0.2 \end{cases} \tag{13}$$

where $Q' = Q/\left(\rho_a C_p T_a g^{1/2} \bar{H}^{5/2}\right)$ denotes the dimensionless heat release rate, and $\bar{H}$ denotes the hydraulic diameter of the tunnel. Using the dimensionless critical velocity obtained from Eq. (13), the physical critical velocity can be calculated from the relationship $u' = u_c/\left(g\bar{H}\right)^{1/2}$.

In the prediction model, the tunnel height was used as the representative length of the tunnel. (Li *et al.* 2010). The equation of the dimensionless critical velocity is then given as

$$u' = \begin{cases} 0.81\left(\dfrac{Q'}{0.2}\right)^{1/3} & Q' \le 0.15 \\ 0.43 & Q' > 0.15 \end{cases} \tag{14}$$

where

$Q' = Q/\left(\rho_a C_p T_a g^{1/2} H^{5/2}\right)$ and $u' = u_c/\left(gH\right)^{1/2}$.

3.2 Smoke Identification

In the FDS, three parameters are used to control smoke production and visibility. The first parameter is the SOOT_YIELD on the REAC line, defined as the fraction of the fuel mass that is converted to soot if a simple chemistry approach is used. In this study, the value of the soot yield was set to 0.1. The second parameter is the MASS_EXTINCTION_COEFFICIENT K_m, which is defined for various light-absorbing gas species. The default value of K_m is $8{,}700\ m^2/kg$, which has been suggested for the flaming combustion of wood and plastics. The third parameter is the VISIBILITY_FACTOR on the MISC line, which is a constant term C, whose default value is 3. Therefore, visibility can be calculated using

$$\mathbf{S = C / K} \tag{15}$$

where C is the constant visibility factor described above, and K represents the light extinction coefficient, which can be expressed as

$$K = K_m \rho Y_s \tag{16}$$

where Y_s is the soot yield and ρY_s denotes the density of the smoke particles.

Vortex Identification: Q_v-Criteria

The Q_v-criterion proposed by Hunt *et al.* (1988) is used to identify a vortex as a connected fluid region with a positive second invariant of the velocity gradient tensor (i.e., $Q_v > 0$). It is intrinsically related to a competition between the vorticity and strain rate where, in the case of a vortex, the vorticity dominates. For incompressible flow, the definition of the Q_v-criterion is given as

$$Q_v = \frac{1}{2}\left(\|\Omega\|^2 - \|S\|^2\right), \quad \|\Omega\|^2 = \mathrm{tr}\left[\Omega\Omega^t\right], \|S\|^2 = \mathrm{tr}\left[SS^t\right] \tag{17}$$

where S and Ω are respectively the symmetric and anti-symmetric components of the velocity gradient tensor ∇U, which are defined as $S = \frac{1}{2}\left[\nabla U + (\nabla U)^t\right]$ and $\Omega = \frac{1}{2}\left[\nabla U - (\nabla U)^t\right]$. Therefore, the competition between the rotation and deformation rates is translated as the difference between the symmetric and anti-symmetric components of the velocity gradient tensor. A vortex is identified where the vorticity dominates the deformation rate.

4. Results and Discussion

4.1 Effect of Window-Breaking of the Car

In the FDS simulation, the car model has four windows with solid glass: the front, rear, left, and right windows. They are considered as solid thin obstructions, which block the free propagation of the flames and air under room temperature and even higher. However, when the temperature of the window reaches a critical value, i.e., $600\ ^\circ C$, abrupt breaking is triggered, which means that the corresponding window will disappear. Figure 4 shows the positions of the four windows and the coordinates of the car.

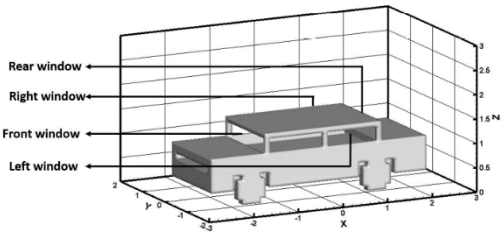

Fig. 4. Detailed configuration of the car model and four windows.

In this study, the burning surface was set to release consistent heat inside the car, which continuously increased the temperature around the windows. Figure 5 shows the variation of the temperature on the four windows with glass. As shown in the figure, it was found that in the case of no ventilation, the front window was broken, but the other three windows remained intact within the simulation time. This is because the two-door windows next to the

driver and passenger seats were opened to provide sufficient oxygen content. Therefore, the temperature around the front window was higher than that around the other three windows. This can also be observed in Fig. 6(a), which shows the contour of the temperature and flow patterns on the XY plane inside the car for $Z = 1.2$.

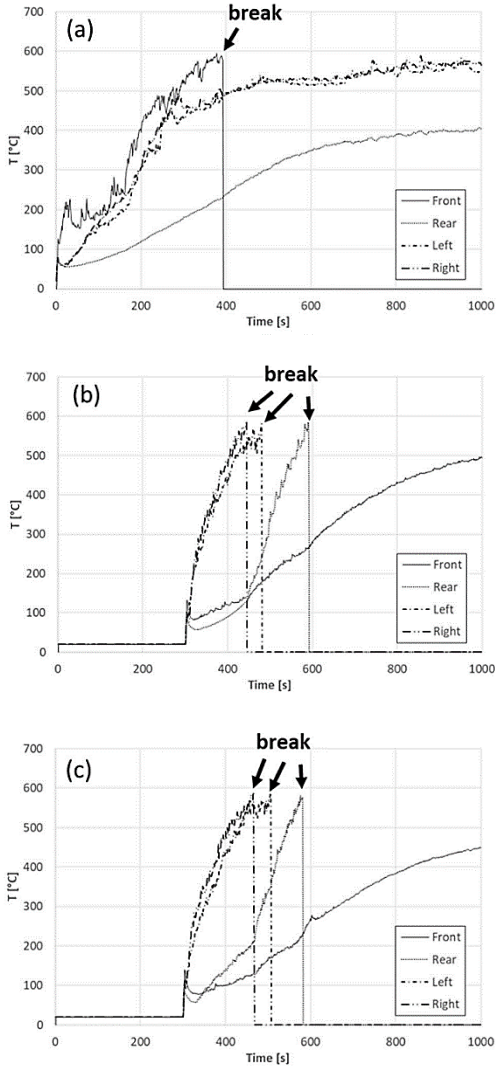

Fig. 5. Temperature variation of the windows of the car: (a) no ventilation; (b) 1.8 m/s ventilation; (c) 3.0 m/s ventilation.

In the ventilation cases (i.e., 1.8 m/s, 3.0 m/s), the fire started after 300 s; before this time, the temperature was maintained similar to an ambient air temperature of 20 $^{\circ}$C . Remarkably, it was found that the rear, left, and right windows were all broken but the front window was not, as shown in Fig. 5(b)-(c). Before the left and right windows were broken, the increasing trend of the temperature on the rear window was similar to that on the front window. However, after these two windows were broken, the temperature on the rear window increased significantly until it reached the breaking temperature. From Fig. 6(b)-(c), it can be observed that the temperature of the rear part of the car was higher than that of the front part. After the left and right windows were broken, external air flowed into the car, which might have had an effect on the temperature increase of the rear window.

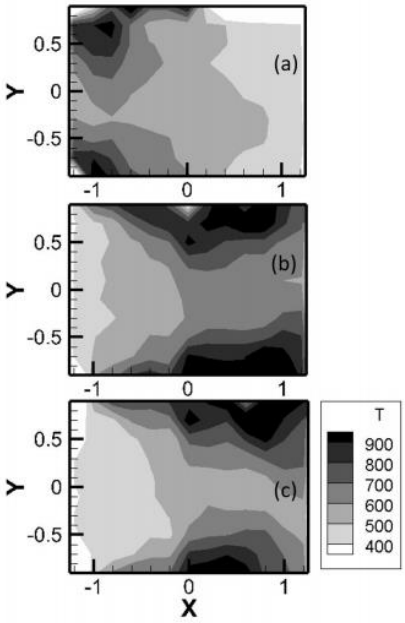

Fig. 6. Contour of temperature on the XY plane for Z = 1:2: (a) no ventilation at 370 s; (b) 1.8 m/s ventilation at 570 s; (c) 3.0 m/s ventilation at 550s.

4.2 Thermo-Fluidic Variation inside the Tunnel

In the absence of natural ventilation, owing to strong thermal buoyancy, the hot air and smoke produced from the car fire rise in its vicinity. When they encounter the solid ceiling of the tunnel, they spread longitudinally in both directions of the tunnel. Figure 7(a) shows the longitudinal velocity profile in the tunnel without natural ventilation. It is also observed that the longitudinal movement of the smoke flow occupies the upper region of the tunnel. Beneath the smoke layer, two streams of air are blown towards the car fire from the two open portals at both ends.

When there is no fire, the longitudinal velocity profile is properly developed as shown in Fig.7. In this case, the car is not burning, and the longitudinal velocity of the natural ventilation is 1.8 m/s. It was found that owing to the effect of viscosity, the longitudinal velocity profiles were similar to the shape of the turbulent boundary layer inside the tunnel, which of course reduces to zero close to the wall. In fact, the wall conditions inside the tunnel correspond to the non-slip boundary condition applied on the tunnel ceiling and floor. Remarkably, the velocity profiles at the inlet region of the tunnel were also observed to have an approximately uniform flow, which became a boundary layer flow when approaching the car and passing it. When the airflow passes over the car, the gradient of the

longitudinal velocity profile increases and rapidly recovers to the boundary layer.

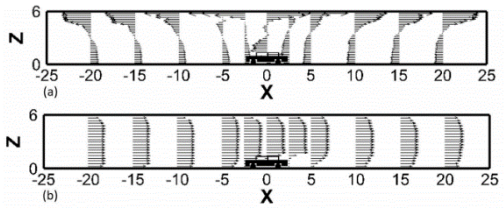

Fig. 7. Longitudinal velocity profiles in the tunnel with (a) ventilation absent; (b) fire absent under natural ventilation of 1.8 m/s.

In general, by combining the two flow pattern types above, the flow around a car on fire under natural ventilation can be effectively obtained. In this case, natural ventilation is expected to propagate the airflow downstream, while the smoke rises to the ceiling of the tunnel owing to the buoyancy-driven flow, ignoring the density difference (i.e., Boussinesq's approximation). Because the smoke spreads bidirectionally in the tunnel, the effect of natural ventilation on the smoke flow is twofold. In the upstream region of the car fire, the ventilation pushes air in a reversed direction to the smoke flow, which reduces the rate at which the smoke spreads in the upstream direction. The presence of the smoke layer in the upstream direction is technically referred to as back-layering. When the back-layering effect is completely suppressed, the corresponding inflow velocity is referred to as the critical longitudinal velocity for natural ventilation. Conversely, in the downstream region of the car fire, the rate at which the smoke spreads increases. Figure 8 shows the flow patterns of the tunnel car fire with two different natural ventilation velocities. It was found that the longitudinal velocity profiles in the upstream and downstream regions of the car fire were distinctive. As shown in Fig.8 (a), the back-layering effect exists in the upstream region of the car fire, which indicates that the critical ventilation velocity is higher than 1.8 m/s. Additionally, when fresh air flows closer to the car fire, its longitudinal velocity component increases slightly because the effective cross-sectional area decreases. For the natural ventilation of 3.0 m/s, the back-layering effect disappears in the upstream region of the car fire, which demonstrates that the critical ventilation velocity is lower than 3.0 m/s. Moreover, the longitudinal velocity profiles almost become the turbulent boundary layer; after passing the car, the profiles are slightly distorted.

Regarding the variation of the temperature field under the car fire, Fig.9 shows the temperature contours after the FDS solution has converged. In the absence of natural ventilation, it was found that a vertical plume always exists and forms a stratified smoke layer that always occupies the upper region of the tunnel, as shown in the figure. Additionally, the structure of the temperature field is symmetrical. In the case of natural ventilation, the plume of the car fire is blown towards the downstream direction, which increases the temperature behind the car. Moreover, the temperature in the upper region of the tunnel is significantly decreased owing to natural ventilation.

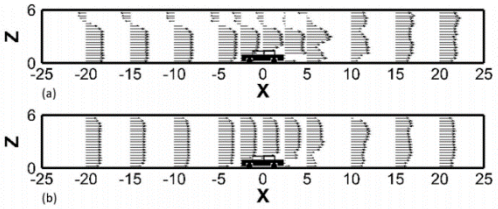

Fig. 8. Longitudinal velocity profiles in the tunnel with car fire: (a) 1.8 m/s ventilation; (b) 3.0 m/s ventilation.

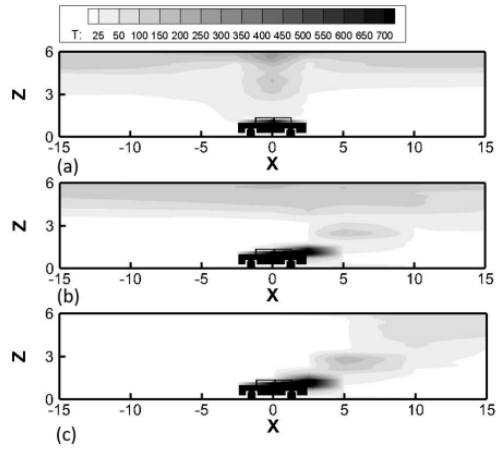

Fig. 9. Contour of temperature in the tunnel: (a) no ventilation; (b) 1.8 m/s ventilation; (c) 3.0 m/s ventilation.

Except for the velocity profile and temperature distribution in the tunnel, the turbulence kinetic energy (TKE) profiles, which are characterized by the root-mean-square velocity, are also calculated. Generally, they can be obtained by the fluid shear, surface friction or buoyancy effect caused by the temperature difference. Figure 10 shows the TKE profiles at various locations in the tunnel when a car catches fire without ventilation. As shown in the figure, the TKE profiles around the car indicate a roughly symmetrical structure in the upstream and downstream regions, which agrees well with the temperature contour (see Fig.9(a)). Additionally, the TKE contour has the highest peak, above the car, and the maximum value under the ceiling of the tunnel. At the symmetrical positions $X = \pm 5$ and ± 10 , the maximum peak value of the TKE profiles at the upstream is slightly higher than that at the downstream. This seems to have been caused by the breaking of the front window in the case without ventilation, which may have caused the fire to spread out and increased the buoyancy effect on the upstream fluid flow.

The symmetrical flow structure would be completely broken if the ventilation flow was considered in the tunnel. As shown in Figs. 11 and 12, the magnitude

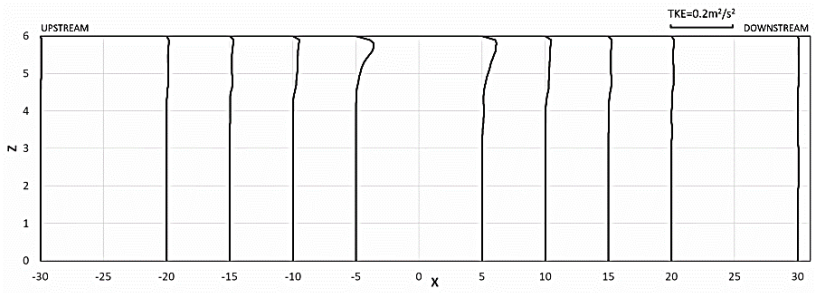

Fig. 10. Turbulence kinetic energy profiles in the tunnel without ventilation: (a) upstream; (b) downstream.

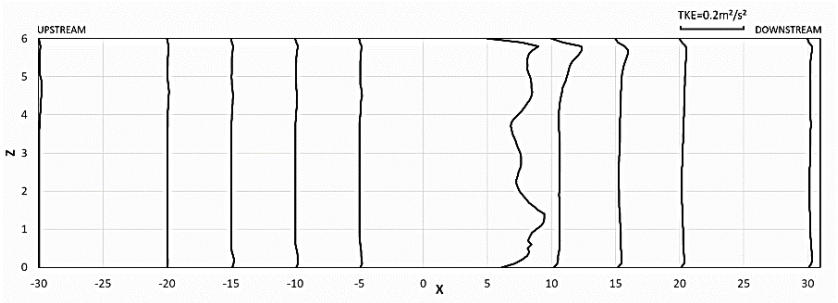

Fig. 11. Turbulence kinetic energy profiles in the tunnel with ventilation 1.8 m/s: (a) upstream; (b) downstream.

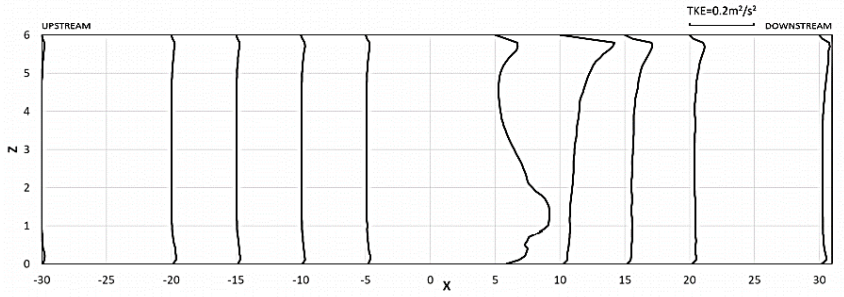

Fig. 12. Turbulence kinetic energy profiles in the tunnel with ventilation 3.0 m/s: (a) upstream; (b) downstream.

of the upstream TKE profile is very low, and its variation along the longitudinal direction is insignificant, whereas it increases at the downstream. In the case of the 1.8 m/s ventilation, the back-layering flow exists at the upstream of the car fire. Except for the positions close to the ground and ceiling of the tunnel, it is found that the magnitude of the TKE profile at the upstream of approximately 4.4 m high is the largest of other positions. This height refers to the position of the interface between the back-layering smoke and fresh air. In that region, the complicated mixing of warm smoke and cool air is substantial, which induces a strong fluctuation of the flow velocity.

Figures 11(b) and 12(b) present the downstream TKE profiles under natural ventilation. Both the smoke and air propagate towards the same direction. The magnitude of TKE at the upper region of the tunnel is higher than that in other regions. However, at the longitudinal position $X = 5$, it is observed that the magnitude of the TKE increases at the lower region of the tunnel. This is caused by the natural ventilation as shown in Fig.9 (b)-(c), which blows the plume of the car fire towards the downstream direction and increases the temperature behind the car.

In this study, the Q_v-criterion was used to identify the vortex structure around the car; we set the value of Q_v as 5. As shown in Fig. 13, it was found that the vortex structures for the no ventilation and ventilation cases are significantly different. Without ventilation, the vortex generation is mainly caused by the effect of thermal buoyancy, which means that the vortices are generated above the car. Additionally, the generated vortices from the car accumulate just beneath the ceiling of the tunnel such that a layer of the vortex structure is formed. Conversely, the effect of natural ventilation should be considered when uniform inflow velocity is

applied at the left portal of the tunnel as ventilation. It is found that the small-scale vortices from the car are mainly from the corners of the car. The vertical vortex structure above the car disappears owing to the ventilation flow.

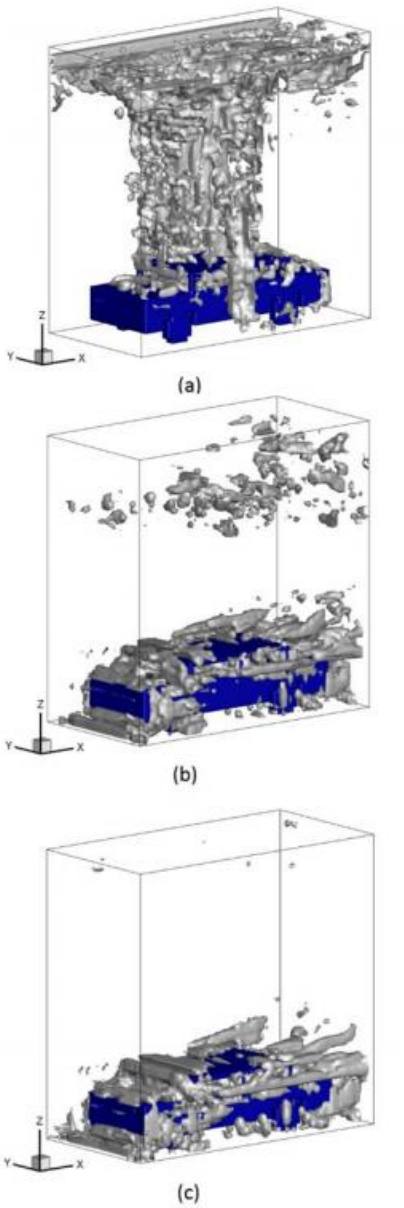

Fig. 13. Iso-surfaces for Qv= 5: (a) no ventilation; (b) ventilation 1.8 m/s; (c) ventilation 3.0 m/s.

4.3 Prediction of Critical Longitudinal Velocity for Natural Ventilation

The FDS simulation is used to predict the critical longitudinal velocity in a tunnel car fire with natural ventilation. Three different velocities (i.e., 1.8 m/s, 2.2 m/s, and 2.3 m/s) for the inflow condition are assigned on the left portal of the tunnel domain. As shown in Fig.14, back-layering occurs in the numerical domain, and the length is significant for the case of 1.8 m/s. When the velocity increases to 2.2 m/s, a small amount of smoke still exists in the upstream region of the car fire. However, when the inflow velocity is 2.3 m/s, a significant amount of the smoke is forced to move in the downstream direction. Therefore, it is concluded that the critical longitudinal ventilation velocity in the current tunnel with a 3.8 MW car fire is approximately 2.3 m/s.

In the simulation, the calculation used 1.172 kg/m^3 and 293 K for the ambient air density and temperature, respectively. Additionally, the specific heat capacity was 1020 $J/(kg \cdot K)$. The simulation was validated in various ways, i.e., typically, by comparing the results of the present study with those from existing studies. One of the parameters we considered was the critical velocity of the longitudinal ventilation, which was also obtained by the semi-empirical models of other researchers, such as Wu and Barkar (2000), Hu *et al*. (2008), and Li *et al*. (2010). The results are presented in Table 1, which includes the existing data. The predicted critical velocity in this study and that of Hu *et al*. (2008) show a good agreement.

Additionally, the predicted critical velocity in this study is slightly higher than that of Li *et al*. (2010). Regarding critical velocity, the model by Wu and Barkar (2000) seems to underestimate the critical velocities obtained by other models.

Table 1 Critical velocities of longitudinal ventilation

Models	$U_c[m/s]$
Wu & Barkar	1.76
Hu *et al*.	2.27
Li *et al*.	2.11
FDS	2.3

5. CONCLUSION

In this study, a set of car fire simulations were presented based on the FDS open-source software package. To effectively control the spread of fire during the car fire simulation, a car model including the body frame, tyres, windows, and other flammable materials was developed. Moreover, the windows were set to be instantly broken when the air temperature around them reached 600 $^{\circ}C$. In the case without ventilation, only the front window was broken, whereas the other three windows were intact. When ventilation was introduced in the tunnel, the left, right, and rear windows were broken and the front window remained intact.

Further, the car fire model was set in a straight two-lane road tunnel to investigate the thermo-fluidic variations around the car. In the tunnel with natural ventilation, it was found that the longitudinal velocity profiles of the upstream and downstream regions of the car fire were distinctive. The temperature in the upper region of the tunnel also significantly decreased owing to natural ventilation.

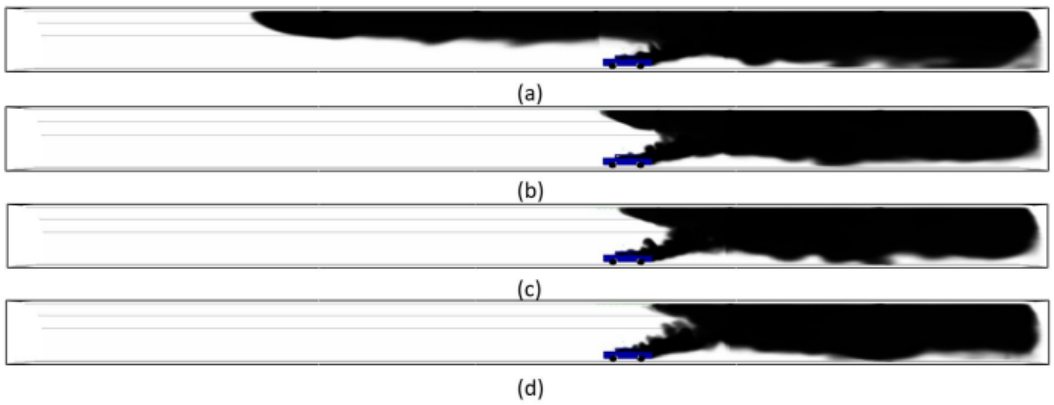

Fig. 14. Smoke patterns inside the tunnel with different ventilation velocities.

A vertical vortex was always generated above the car in the absence of ventilation; conversely, the vertical vortex structure disappeared in the case with ventilation, and small-scale vortices were generated mainly from the corners of the car. In the case of natural ventilation, the magnitude of the upstream turbulence kinetic energy was very low compared with that of the downstream. Regarding the vortex structure around the car in the case without natural ventilation, vertical vortices were generated above the car. Conversely, no vertical vortices were generated under natural ventilation conditions, and small-scale vortices were formed mainly from the corners of the car.

For the tunnel car fire with a specific HRR (i.e., 3.8 MW) and natural ventilation, the critical longitudinal velocity always exists, which is required to suppress back-layering flow in the tunnel. In this work, the FDS was applied to predict this critical velocity by conducting several simulations with different steady inflow velocities. The critical longitudinal velocity was found to be approximately 2.3 m/s. Additionally, some semi-empirical models were also provided to estimate the critical velocity of the tunnel car fire with a maximum HRR of 3.8 MW. The results of the FDS simulation showed good agreement with the results predicted using the semi-empirical model proposed by Hu *et al.*

6. ACKNOWLEDGEMENTS

This work was supported by `Human Resources Program in Energy Technology' of the Korea Institute of Energy Technology Evaluation and Planning (KETEP), granted financial resource from the Ministry of Trade, Industry \& Energy, Republic of Korea (no. 20164030201230). In addition, this work was supported by the National Research Foundation of Korea (NRF) grant funded by the Korea government (MSIP) (no. 2019R1I1A3A01058576). This work was also supported by the National Supercomputing Center with supercomputing resources including technical support (KSC-2020-INO-0025)

REFERENCES

Atkinson, G. and Y. Wu (1996). Smoke control in sloping tunnels. *Fire Safety Journal 27*, 335–341.

Beard, A. (2009). Fire safety in tunnels. *Fire Safety Journal* 44, 276–278.

Beard, A. and R. Carvel (2005). *The Handbook of Tunnel Fire Safety*. London, UK: Thomas Telford.

Deardorff, J. (1980). Stratocumulus-capped mixed layers derived from a threedimensional model. *Boundary-Layer Meteorology* 18, 495–527.

Hong, W. (2004, March). The progress and controlling situation of daegu subway fire disaster. In *6th Asia-Oceania Symposium on Fire Science and Technology*, Daegu, Korea.

Hu, L., R. Huo and W. Chow (2008). Studies on buoyancy-driven back-layering flow in tunnel fires. *Experimental Thermal and Fluid Science* 32, 1468–1483.

Huang, H., S. Kato, R. Ooka and T. Jiang (2006). Cfd analysis of ventilation efficiency around an elevated highway using visitation frequency and purging flow rate. *Wind and Structures* 9, 297–313.

Hunt, J., A. Wray and P. Moin (1988, December). Eddies, streams, and convergence zones in turbulent flows. In *Center for Turbulence Research - Proceedings of the Summer Program*, California, USA.

Hwang, C. and J. Edwards (2005). The critical ventilation velocity in tunnel fires – a computer simulation. *Fire Safety Journal* 40, 213–244.

Ingason, H., Y. Z. Li and A. Lonnermark (2015). *Tunnel Fire Dynamics*. New York, USA: Springer.

Iqbal, Q. and A. Chan (2016). Systematic influence of wind incident directions on wind circulation in the re-entrant corners of high-rise buildings.

Wind and Structures 22, 409–428.

Jones, J., M. McMullen and J. Dougherty (1987). Toxic smoke inhalation: cyanide poisoning in fire victims. *American Journal of Emergency Medicine* 5, 317–321.

Kim, H. K., A. Lonnermark, H. Ingason (2010). *Effective fire fighting operations in road tunnels*. Boras, SWEDEN: Fire Technology SP Report.

Kurioka, H., Y. Oka, H. Satoh and O. Sugawa (2003). Fire properties in near field of square fire source with longitudinal ventilation in tunnels. *Fire Safety Journal* 38, 319–340.

Lee, S. and H. Ryou (2006). A numerical study on smoke movement in longitudinal ventilation tunnel fires for different aspect ratio. *Building and Environment* 41, 719–725.

Leitner, A. (2001). The fire catastrophe in the tauern tunnel: experience and conclusions for the austrian guidelines. *Tunnelling and Underground Space Technology* 16, 217– 223.

Li, Y., B. Lei and H. Ingason (2010). Study of the critical velocity and backlayering length in longitudinally ventilated tunnel fires. *Fire Safety Journal* 45, 361–370.

Liu, C., M. Zhong, X. Tian, P. Zhang and S. Li (2019). Study on emergency ventilation for train fire environment in metro interchange tunnel. *Building and Environment* 147, 267– 283.

McGrattan, K., S. Hostikka, R. McDermott, J. Floyd, C. Weinschenk and K. Overholt (2013). *Fire Dynamics Simulator (Version 6.4.0) User Guide*. NIST, USA.: NIST Special Publication.

Muhic, S. and M. Mazej (2014). Computational study of road tunnel exposure to severe wind conditions. *Wind and Structures* 19, 185– 197.

Oka, U. and G. Atkinson (1995). Control of smoke flow in tunnel fires. *Fire Safety Journal* 25, 305–322.

Rehm, R. and H. Baum (1978). The equations of motion for thermally driven, buoyant flows. *Journal of Research of the NBS* 83, 297–308.

Rew, C. and D. Deaves (1999). Proceedings of tunnel fires and escape from tunnels. In *Fire spread and flame length in ventilated tunnels, a model used in channel tunnel assessments*, Lyon, France.

Thomas, P. (1968). The movement of smoke in horizontal passages against an air flow. *Fire Research Notes*, 723.

Vuilleumier, F., A. Weatherill and B. Crausaz (2002). Safety aspects of railway and road tunnel: example of the lotschberg railway¨ tunnel and mont-blanc road tunnel. *Tunnelling and Underground Space Technology* 17, 153–158.

Wen, J., K. Kang, T. Donchev and J. Karwatzki (2007). Validation of fds for the prediction of medium-scale pool fires. *Fire Safety Journal* 42, 127–138.

Weng, W., X. Lu, F. Liu, X. Shi and L. Yu (2015). Prediction of backlayering length and critical velocity in metro tunnel fires. *Tunnelling and Underground Space Technology* 47, 64–72.

Wu, Y. and M. Barkar (2000). Control of smoke flow in tunnel fires using longitudinal ventilation systems – a study of the critical velocity. *Fire Safety Journal* 35, 363–390.